*Applications of NMR Spin Imaging to the Study of Lungs**

D. C. Ailion, T. A. Case, D. D. Blatter, A. H. Morris, A. G. Cutillo, C. H. Durney, and S. A. Johnson

Departments of Physics, Medicine, Electrical Engineering and Bioengineering
University of Utah
Salt Lake City, Utah 84112

I. INTRODUCTION

Cardiopulmonary diseases are responsible for more than three million hospitalizations and 30,000 deaths yearly in the United States alone. Changes in lung water content or distribution are associated with virtually all pulmonary disorders. The development of noninvasive methods for measuring lung water and its distribution could have major impact upon evaluation of edematous states of the lung, such as adult respiratory distress syndrome (ARDS) and heart failure; states with altered lung density, such as pulmonary fibrosis and emphysema; and cardiac disorders associated with increased left atrial pressure (with increased pulmonary vascular volume but without lung edema). It is thus of obvious medical importance to develop methods for measuring the total water in the lung as well as its spatial distribution.

Existing non-NMR methods (1) for measuring lung water typically involve destructive or invasive techniques (double-indicator dilution, histologic, and gravimetric), depend on regional distribution of pulmonary vascular perfusion (blood flow in the arteries and veins of the lung; e.g., the double-indicator dilution technique) and regional distribution of ventilation (amount of air flow in the lung; e.g., the inert gas rebreathing technique), or involve harmful radiation (X-ray or isotopic double-indicator dilution). Most of these techniques measure only a *fraction* of the total water in the lungs rather than the total water. Furthermore, the distribution spaces of the various indicators differ and are poorly defined.

NMR has obvious advantages in that it is noninvasive and nondestructive and clearly has the capability of *quantitative* determination of *total* lung water. NMR imaging has the further advantage of being able to determine regional abnormalities and, thus, the relationship between the appearance of these abnormalities and the occurrence of disease. NMR imaging is particularly well suited to time-course studies of the development of disease.

There are a number of difficulties in NMR imaging of lungs. First, the water density (and thus the signal-to-noise ratio) will be lower in lungs than in other tissue. A related problem is the effect of nearby water (either due to the chest wall or to pockets of water near the lung). It is a nontrivial problem just to define the boundaries of the lung in the edematous state. A second problem is that the lung image may be blurred by lung movement during breathing. This problem can be solved by breath holding or by gating the NMR signal from the respiratory cycle. If the chest motion can be constrained externally, the lung motion may be kept within acceptable bounds. A further problem, as we shall see later in this paper, arises from the fact that lung is a highly aerated organ with a large surface-to-volume ratio.

Our initial work has concerned validation of NMR methods for quantitative lung water measurement. By comparing the NMR results with results from standard gravimetric techniques, NMR can be shown to provide an absolute standard for the determination of total lung water content, changes in which can be used to study lung disease. Even though an NMR image may be well-defined, its validation is nontrivial. It is difficult to cut away sections of the lung for subsequent gravimetric measurements without causing irreversible changes in the tissue (due, for instance, to collapse of the lung and changes in fluid content). As a result, one does not know

---

*Presented at the 6th Specialized Colloque Ampere on "Quadrupole Interactions and Spatially Resolved NMR in Solids," Crete, Greece, September 12-17, 1983.

a priori which gravimetric sections correspond to which NMR pixels. Another source of error in performing *absolute* NMR measurements arises from the need to perform extrapolation of the spin-echo envelope to correct for the T_2-decay of the magnetization. For selective NMR irradiation, pulses are needed whose widths may be several milliseconds. An incorrect determination of the time of the beginning of the magnetization decay may result in errors of 10 to 15% in the determination of the thermal equilibrium magnetization M_0.

A second application of NMR imaging is to study the time course development of pulmonary edema (accumulation of fluid in the lungs). In particular, NMR imaging might detect spatial patterns of lung edema as well as changes in these patterns associated with exposure to different toxins and diseases.

A third purpose of our study is to use NMR imaging to determine the state of aeration of the lungs as well as to study possible effects of oxygen toxicity.

II. LINE-SCAN TECHNIQUES

The experiments described in this paper were performed in a 12" Varian electromagnet designed for broad-line solid-state physics. Because of the limited size of the homogeneous region in this magnet (approximately 20 cm^3 sample volume for ± 0.1 Gauss), we use a line scan technique in which we observe only a narrow, pencil-shaped region located in the center (homogeneous region) of the magnet. We then sequentially step the specimen (in our case, a small rat) up or down and repeat the line scan. In this way a two-dimensional picture is obtained from a series of one-dimensional line scans, each of which arises only from nuclei in the homogeneous region.

A line scan (2) is obtained by selective excitation (i.e., using gradients and narrow frequency pulses) of two perpendicular planes, the first with a 90° pulse and the second with a 180° pulse. Thus, only their region of intersection (the shaded region of Figure 1) will have received *both* a 90° and a 180° pulse. A pulse sequence for achieving a line scan is shown in Figure 2. The z-gradient (applied only during the 90° pulse) guarantees that the 90° pulse excites only a planar region corresponding to a particular z-value whereas the y-gradient guarantees that only a particular y-plane sees the 180° pulse. Thus, only the "line" having a particular y- and z-coordinate will experience both pulses and will contribute to the spin-echo (shown in the lowest trace of Figure 2). The application of an x-gradient (turned off during the 90° and 180° pulses to allow definition of the y- and z-planes) allows separation of data along the x-direction. (Several refinements of this simple sequence which are needed to correct for effects such as dephasing during the gradient pulses and dephasing due to field inhomogeneities will be discussed in a subsequent paper (3).)

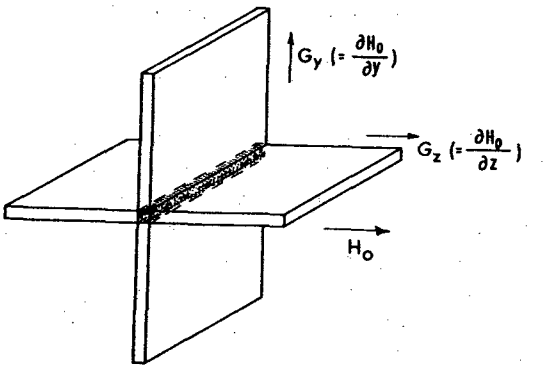

Figure 1. Intersecting planes used in the line-scan technique.

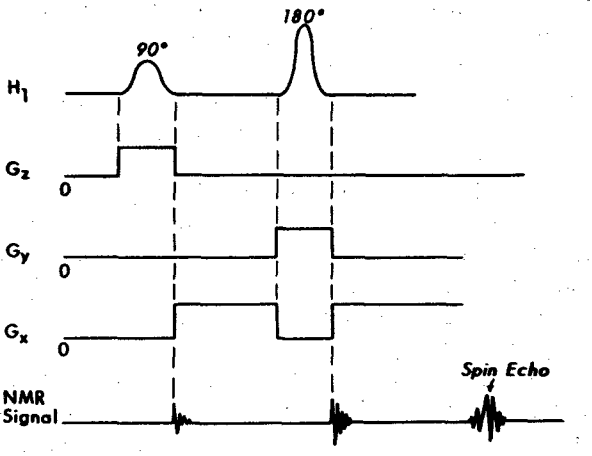

Figure 2. Pulse sequences used in the line-scan technique.

III. VALIDATION OF NMR MEASUREMENTS IN LUNG

In order to obtain accurate quantitative determination of the water content in lung from the spin-echo amplitude, it is necessary to correct for the T_2 decay of the signal which occurred prior to the occurrence of the spin echo. A suitable back extrapolation can be obtained by varying the time interval between the 90° and 180° pulses. We obtained our data for two such intervals (11 ms and 19 ms) and formed an image after fitting this data to a single exponential which was then back-extrapolated to the center of the first pulse. (The justification for this procedure is discussed more fully in another paper(4).) We obtained the percentage water in each pixel of the image by dividing the lung magnetization pixel-for-pixel by the magnetization obtained for pure water which was previously placed in the same region.

In lung it is difficult to make a comparison between the water density of a small portion of the lung measured by NMR with that measured gravimetrically. The difficulty begins when one opens the chest cavity to obtain a lung fragment corresponding to an area in the NMR image. At this point the lung collapses, and one can no longer identify the specific lung tissue which generated any particular NMR signal in the image. Further, if one were to cut the lung, fluids that were imaged might leak out of the fragment and thus not be measured gravimetrically.

Our solution to this problem is to remove the lungs surgically: tying off the major blood vessels to retain close to normal physiological fluid content and then inserting a tube into the trachea so that the lungs could be kept in a steadily inflated state by an external air pressure supply. This preparation is then inflated snugly into a rectangular jig (see Figure 3) with small vials of water on either side for position reference. Then the entire jig is scanned until NMR images are collected from the entire volume. After imaging, the still inflated lung in the jig is removed from the magnet and rapidly frozen in liquid nitrogen to preserve the geometry and water content of all parts of the lung and jig. The frozen lung within the jig is then separated from the remainder of the lung and sectioned into 1.9 mm slices perpendicular to the long axis of the jig. The relation of each section to the reference vials of water is noted so that a correlation can be made between the frozen lung sections and the corresponding NMR image signals. The lung sections are then weighed and allowed to dry to

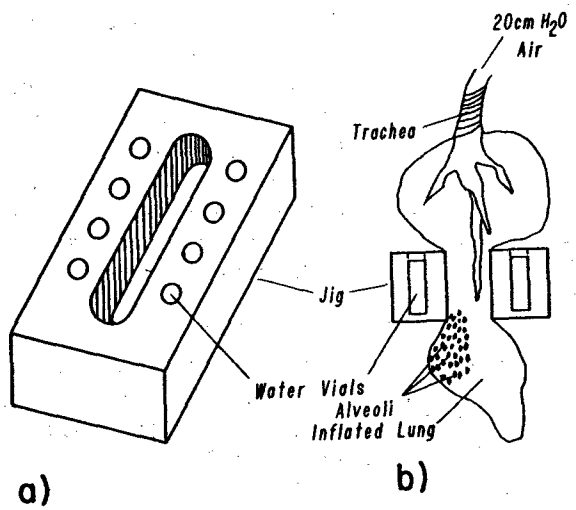

Figure 3. Jig used for validation studies. (a) Jig. (b) Cross-sectional view of jig with lung.

constant weight in an oven at 60° C, thereby providing an absolute gravimetric measure of the water in the region.

IV. INHOMOGENEOUS BROADENING CONTRAST TECHNIQUE (T_2')

A. Diamagnetic Line Broadening

In the process of performing the validation experiments described above, we discovered some surprising effects which led us to a new method for doing NMR imaging. In particular, we have observed that the NMR line of inflated lung is inhomogeneously broadened by an internal broadening mechanism (in contrast to external field inhomogeneities). Since this effect is not observed in most other tissues (other than fat), it has resulted in a new high-contrast technique for imaging lungs and fat.

Figure 4 show free induction decays (FID's) obtained from an inflated lobe of rat lung (Figure 4a) and from pure water (Figure 4b) in a relatively homogeneous field (i.e., no external gradients). Both samples had the same volume and were located in the same position in the magnet. As we can see from Figure 4b, T_2^* of the water is of order 18 ms in this magnetic field, thereby defining the broadening due to the *external* field inhomogeneity. Since T_2^* of the lung is only approximately 4 ms in the same field, the lung is

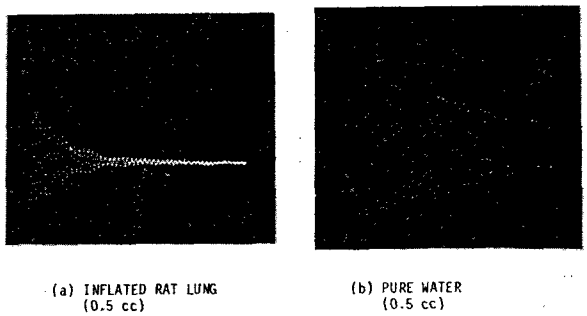

Figure 4. Free induction decays, (a) inflated rat lung (0.5 cc) and (b) pure water (0.5 cc). The time scale is 25 μs/pt or 13.6 ms for the entire horizontal sweep.

experiencing an extra broadening mechanism which cannot be due to external field inhomogeneities. We found that, if the same lobe of lung is subjected to a Carr-Purcell sequence, T_2 (25-30 ms) will be much longer than T_2*. Thus, the extra broadening mechanism experienced by the lung must be inhomogeneous broadening, but not due to inhomogeneities in the external field. Our evidence, as we shall see, is that the source of this internal magnetic field inhomogeneity in lung arises from different diamagnetic shifts experienced by water molecules at different distances from the lung surface (air-water interface).

Since water and most tissues are slightly diamagnetic (5), the proton resonance in liquid water is shifted by approximately 360 Hz in a 40 MHz NMR imaging apparatus. In a tissue specimen which is homogeneous across the resolution size, all protons in a pixel (though frequency shifted) will remain in phase with one another and the magnitude of the signal will not decrease. However, if the diamagnetism of the tissue is inhomogeneous, as in lung tissue which consists of a foam-like mixture of water and air, the protons within a pixel will precess with different frequencies (those near an air space being in a higher field than those deeper within the tissue).

If this interpretation is correct, it should be possible to simulate similar broadening and line shifts in other substances having boundary surfaces between regions of sharply different diamagnetic susceptibility. Accordingly, we performed measurements of the NMR lines in foams (air-water interface) and in a dense slurry of alumina particles (alumina-water interface). The diamagnetic susceptibility of alumina is approximately twice that of water. Thus, the resonance of water molecules at an alumina-water interface should exhibit a shift of approximately the same order of magnitude as those at an air water interface but of opposite sign. *of opposite sign.* Figure 5a shows the narrow line of a sample of water containing the detergent Joy™. This sample was then agitated to produce a foam, which has many air-liquid interfaces and exhibits line broadening (Figure 5b). We observed a similar line broadening in shaving cream (Figure 5c). Note that that the process of producing air-water interfaces causes a broadening and shift similar to that which is observed in lung. The results of a critical test as to whether this broadening and shift arises from surface diamagnetic susceptibility variations is shown (in Figure 5d) for a water-alumina slurry. This figure shows that the shift is indeed of opposite sign but comparable order of magnitude to that of the foam and shaving cream. We have thus shown that air-water interfaces can provide line broadening and shifts similar to that of lung and that this broadening and these line shifts may be varied by changing the diamagnetic susceptibility mismatch.

B. Technique for Observing Internal Inhomogeneity Effects on Spin Echo

As we stated earlier, our line-scan images involve refocusing of the magnetization into a spin echo. Since this spin echo involves a refocusing of the magnetization lost from all inhomogeneities (both internal and external), the question arises as to how we can see the effects of the internal broadening (described above) in an image formed from spin echoes. We now describe our technique for observing a new kind of spin echo: one in which only the signal lost from gradients (but not internal or external inhomogeneities) is refocused. The error due to loss of signal from external inhomogeneities can be corrected by use of a normalizing curve obtained from the signal intensity arising from a bucket of pure water placed in the same spatial region of the magnet.

First consider a 90°-180° pulse sequence applied without field gradients. At 2τ we obtain a conventional spin echo, where τ is the time between the 90° and 180° pulses. the width of the echo defines an inhomogeneity window

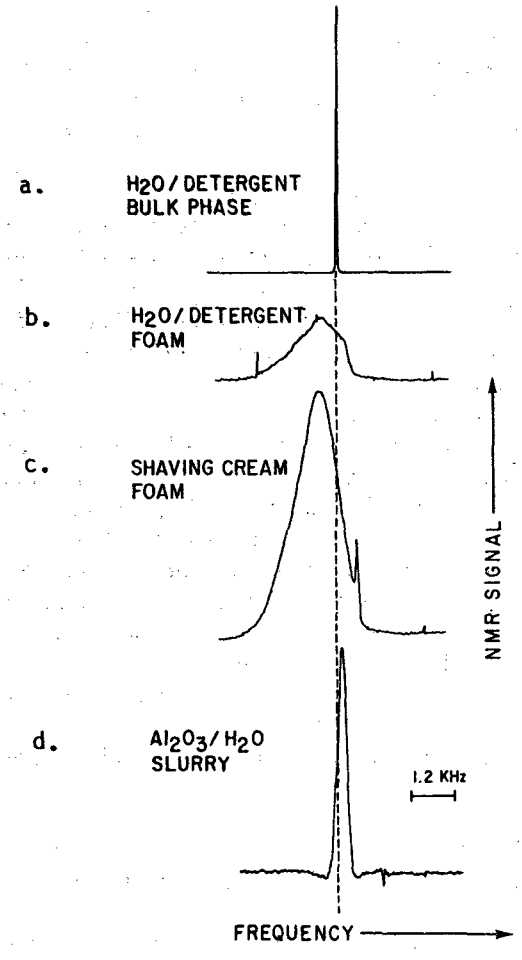

Figure 5. NMR lines for mixtures of substances having different diamagnetic susceptibilities.

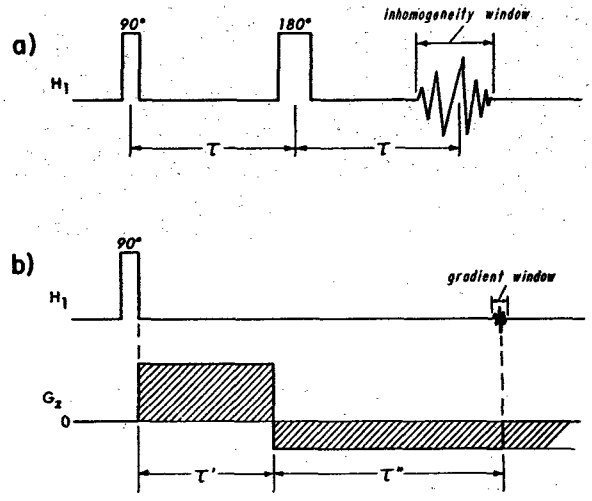

Figure 6. Two different kinds of spin echoes. (a) The conventional echo obtained from a 90°-180° sequence; and (b) the echo obtained from reversing the dephasing in a gradient. The echo will occur when the area under the curve when G_z is negative equals the area when G_z is positive.

(Figure 6a) in which it is possible to have a signal for a given value of τ. Similarly, if a gradient is applied following a 90° pulse, there will be rapid dephasing which will be reversed simply by reversing the direction of the gradients. An echo, whose width depends both on the sample and on the size of the gradients, will occur at $\tau' + \tau''$ when the total *area* under the gradient curve is zero (i.e., when the positive area equals the negative area in Figure 6b). If the positive and negative gradients are equal in magnitude, then $\tau'' = \tau'$, and the sequence is described as symmetric. However, if the gradients are unequal, $\tau'' \neq \tau'$, and the sequence is called asymmetric; thus the position of the gradient echo can be adjusted simply by varying the relative amplitudes of the two gradients. Furthermore, it should be noted that the width of the gradient echo of Figure 6b normally will be much less than that of the inhomogeneity echo of Figure 6a since it corresponds to a signal in a much more inhomogeneous field (that of the gradient). Now, if a 180° pulse is applied precisely at τ' (so that $\tau' = \tau$) and the second gradient is not reversed in sign, all the signal lost from inhomogeneities (both internal and external) is refocused and the maximum echo amplitude will have decayed from M_0 at a rate determained by T_2. This sequence (i.e., when the gradient following the 180° pulse is equal in amplitude and sign to the gradient following the 90° pulse) is clearly symmetric in that $\tau' = \tau'' = \tau$. In this case the gradient and inhomogeneity windows are centered at the same point in time, $\tau' + \tau'' = 2\tau$

and the maximum possible spin echo will appear at the center of the inhomogeneity window (see Figure 7a). However, if the second gradient is

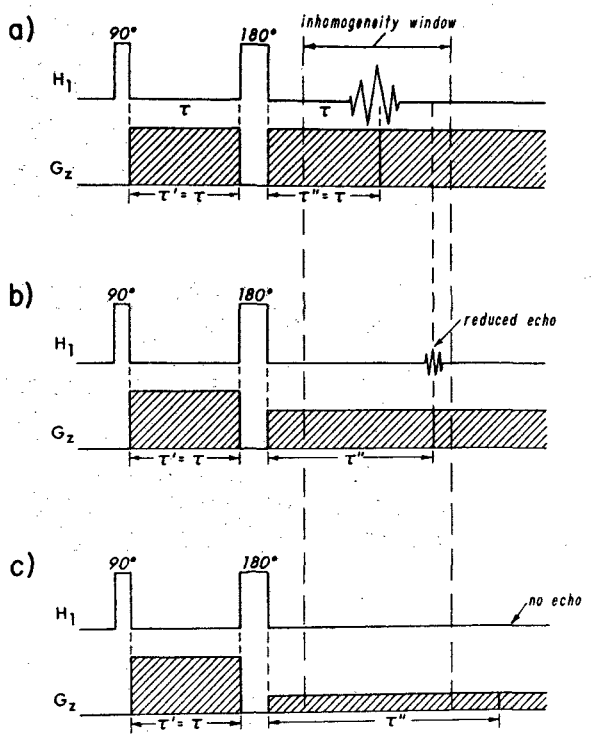

Figure 7. Effect of symmetric and asymmetric sequences. (a) Symmetric sequences. (b) Asymmetric sequences with partially overlapping windows and reduced echo. (c) Asymmetric sequences with no overlap of windows and zero echo.

reduced somewhat (so that $\tau'' \neq \tau'$ and the sequence is asymmetric), we will get a reduced echo if the τ'' interval ends within the inhomogeneity window (as in Figure 7b) or no echo if τ'' ends outside the inhomogeneity window (as in Figure 7c). This reduction in signal intensity can be understood by recognizing that, with unequal gradients, the signal loss due to external gradients is refocused at a different point in time than is the signal loss due to internal inhomogeneities. Thus, only part of the signal lost from internal inhomogeneities has been refocused at the point of optimal refocusing for the signal lost from external field gradients (i.e., center of gradient window). Figure 8 indicates a possible envelope of the inhomogeneity window generated by asymmetric sequences having different sized

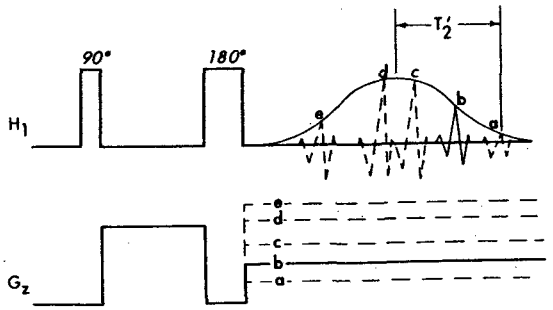

Figure 8. Shape of inhomogeneity window determined by echoes generated by a series of gradients of unequal amplitude.

gradients. The width of the inhomogeneity window in the absence of external gradients is approximately $2T_2^*$. However, for a perfectly homogeneous external field or for a sample (like lung) in which internal inhomogeneities determine the magnetization dephasing, the width of the window is $2T_2'$, where T_2' is defined as the FID decay time due to internal inhomogeneities (i.e., for a perfectly homogeneous external field assuming negligible contributions from T_2, as described below).

We can understand in another way why the spin-echo amplitude is reduced for the asymmetric sequence when internal inhomogeneities are present. If we assume that different line-broadening mechanisms independently give rise to exponential decay of the FID, we can write the total FID decay rate, $1/T_2^*$, as a sum of contributions from different mechanisms,

$$1/T_2^* = 1/T_{2,g} + 1/T_{2,m} + 1/T_2' + 1/T_2 , \quad (1)$$

where $1/T_{2,g}$, $1/T_{2,m}$, $1/T_2'$, and $1/T_2$ are, respectively, the contributions to the broadening from external field gradients, inhomogeneities in the static magnetic field H_0, internal sources of field inhomogeneity, and irreversible sources. In a liquid, normally, $T_2 >> T_{2,m}$, $T_{2,g}$. Since dephasing from irreversible sources is not refocused to a spin echo, the decay of the spin-echo magnetization from its peak value is given by

M =

$$M_p \exp[-t(1/T_{2,g} + 1/T_{2,m} + 1/T_2')], \quad (2)$$

where

$$M_p = M_0 \exp(-\tau''/T_2). \quad (3)$$

For the simple 90°-180° pulse sequence of Figure 6a, the $1/T_{2,g}$ term is absent (since there are no external gradients). For aerated rat lung in our iron magnet, $T_{2,m} >> T_2'$, since $T_2' \sim 4$ ms and $T_{2,m} \sim 18$ ms, as we have seen in Figure 4. Thus, the echo envelope in the absence of gradients (the inhomogeneity window) is determined primarily by T_2' and the magnetization decay of the echo is given by

$$M \simeq M_p \exp(-t/T_2'). \quad (4)$$

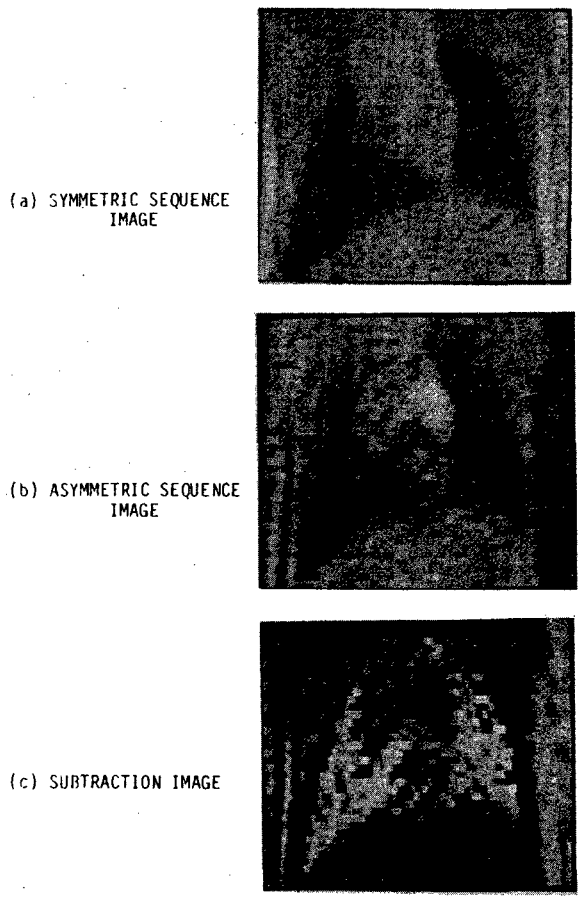

Figure 9. Thorax of dead intact rat. (a) Symmetric sequence image. (b) Asymmetric sequence image. (c) Subtraction image.

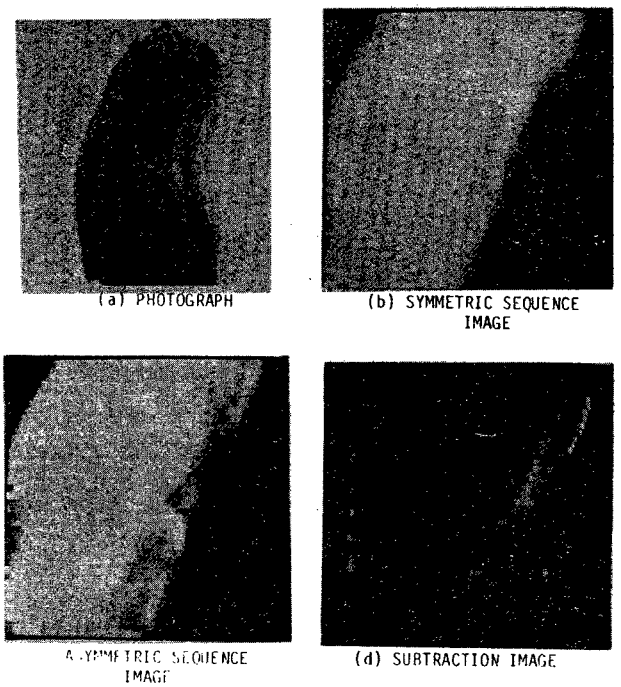

Figure 10. Human kidney. (a) Photograph. (b) Symmetric sequence image. (c) Asymmetric sequence image. (d) Subtraction image.

Now, in the presence of external gradients, we must include the $T_{2,g}$ term, in which case the echo width is determined by $T_{2,g}$, since $T_{2,g} << T_2$. The amplitude of the spin echo is determined by its position in the inhomogeneity window, as shown in Figure 8.

V. RESULTS

It is clear from the previous discussion that a T_2' image can be generated simply with an asymmetric imaging sequence (utilizing unequal gradients). If the gradient and inhomogeneity windows partially overlap, there will be a reduced signal due to internal inhomogeneity effects. If, on the other hand, a symmetric sequence is used so that the echo occurs in the center of the inhomogeneity window, there will be no loss in signal intensiy, and we will get a conventional proton density image. If we subtract the asymmetric from the symmetric image pixel-by-pixel, we will obtain an image of *only those* nuclei which experience internal broadening

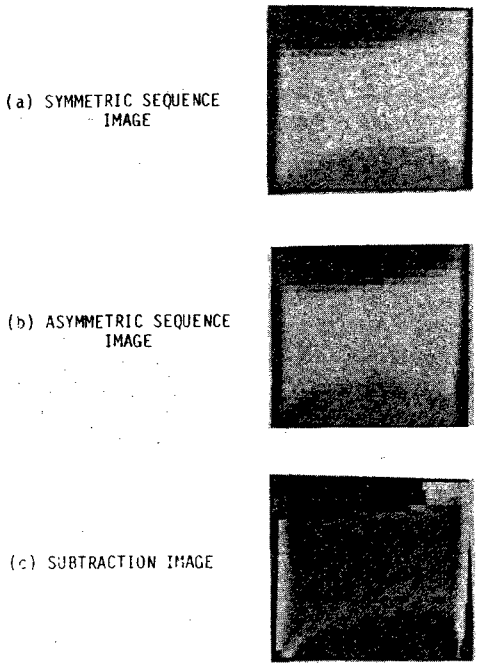

Figure 11. Salad oil floating on water. (a) Symmetric sequence image. (b) Asymmetric sequence image. (c) Subtraction image.

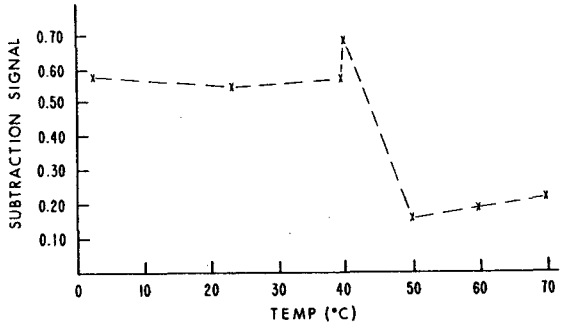

Figure 12. Temperature dependence of the relative intensity of the subtraction image in Crisco™. The subtraction signal intensity is expressed as a percentage of the normal signal intensity obtained with the symmetric sequence.

(like protons in lung). In such an image, regions containing protons but no internal broadening (like bulk water) will be dark as will regions containing no nuclei. Only those nuclei experiencing internal broadening will appear in the image. We now present a number of images which demonstrate the effect.

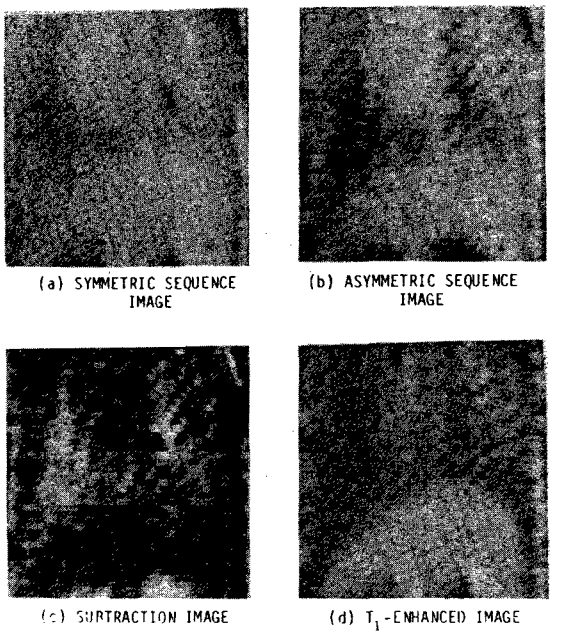

Figure 13. Pulmonary edema in dead rat. (a) Symmetric sequence image. (b) Asymmetric sequence image. (c) Subtraction image. (d) T_1-enhanced image.

Figure 9 shows the thorax of a dead intact rat. Figures 9a and 9b show the results with symmetric and asymmetric sequences, respectively. Note, in both cases the lungs are dark (due to their relatively low water content). In contrast, in the subtraction image, Figure 9c, the lungs appear bright whereas other regions appear dark (including the chest wall). However, it should be noted that some other regions also appear bright (e.g., the bright regions outside the lung on the right and on the left side of the pictures). We believe these regions to be fatty tissue, which also is intensified by our contrast technique.

Figure 10 shows a photograph of a piece of a human kidney (Figure 10a) as well as the three NMR images. Note that, in the subtraction

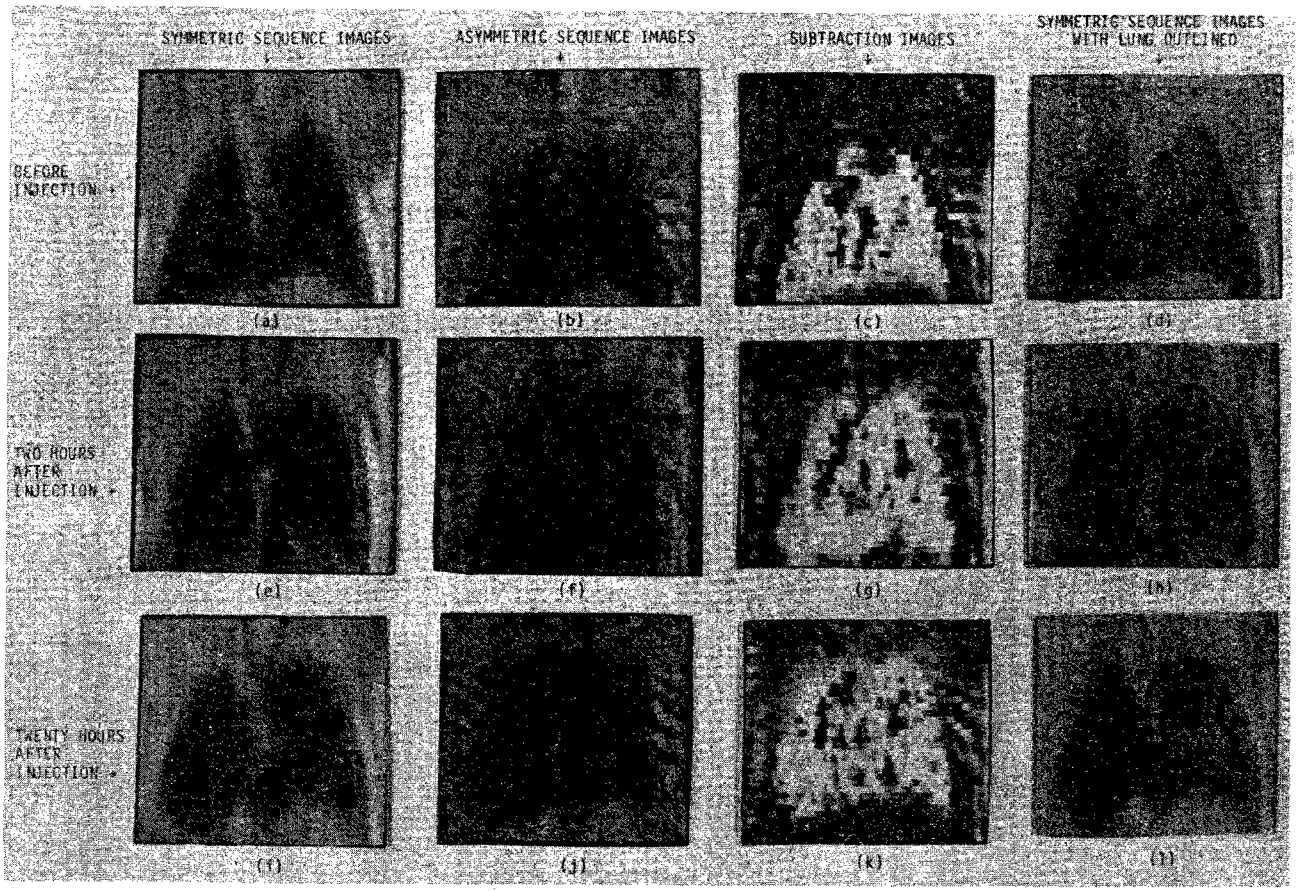

Figure 14. Oleic acid-induced lung edema in a live rat.

image (Figure 10d), the fatty region on the right (perihilar fat) as well as the surface regions are intensified.

In order to attempt to understand the mechanism for internal T_2' broadening in fat, we obtained images of liquid salad oil floating on water (Figure 11). Both liquids show up in our symmetric and asymmetric pictures (Figures 11a and 11b), but only the salad oil appeared in the difference image, thus demonstrating that even a fatty liquid will be contrasted by our technique. We also measured the temperature dependence of the relative intensity of the difference image in hydrogenated vegetable oil (Crisco™) which is "solid" up to approximately 48 °C and then melts. As shown in Figure 12, there is a sharp reduction in the intensity and thus in the internal broadening in the liquid. Thus we conclude that the internal broadening mechanism in fat arises from at least two sources, one of which is motionally narrowed upon melting and possibly is due to dipolar interactions. The mechanism in the liquid oil probably involves protons at different chemically shifted sites. This point will be discussed further in a subsequent paper (6). Since our contrast technique appears to work in *bulk* fat, it is clear that the mechanism for internal broadening here must be quite different from the diamagnetic susceptibility mismatch at the air-water interface in lung.

Figures 13 and 14 show the effects of edema (7) on the lungs of intact rats. In both cases, the lung edema was caused by 0.04 mL of oleic acid injected via the lateral tail vein. The rat in Figure 13 died, whereas the rat in Figure 14 survived. In the conventional proton density image (using a symmetric sequence) in Figure 13a the edema is so widespread that it is nearly impossible to distinguish the boundaries of the lung from the surrounding tissues. However, the difference image of Figure 13c shows the boundary of the lung quite clearly. The T_1-enhanced image of Figure 13d offers some contrast for the lung, but much more for the liver (the bright region at the

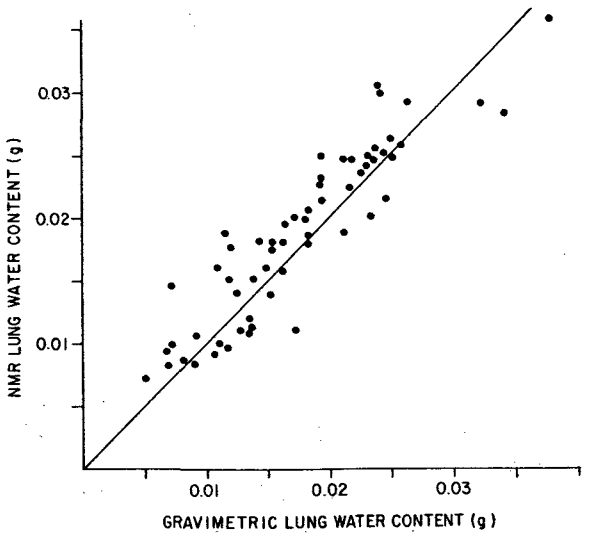

Figure 15. Validation study of NMR lung water measurements.

bottom of the photograph). This set of images shows an important application of our T_2' technique: that of determining the boundary of the lung in the presence of massive edema.

Figures 14a-l show three sets of images taken on a live spontaneously breathing rat, also subjected to oleic acid injection. The first set of four pictures (Figures 14a-d) was taken before the intravenous oleic acid injection, the second set (Figures 14e-h) was taken two hours after the oleic acid injection, and the third set (Figures 14i-l) was taken the next day, 20 hours after the injection. Figure 14e shows clearly the onset of edema in the right lower lobe and the difficulty in determining the lower boundary of the lobe (which is easily determined with an asymmetric sequence in Figure 14f and in the subtraction picture of Figure 14g). In Figure 14i-l taken the next day, there is partial resolution of lung edema but the appearance of a pleural effusion. Note that the difference between lung edema and pleura effusion is indicated in the subtraction image. It is also interesting to note in Figure 14g the persistence of bright regions even in areas of significant edema, indicating the maintenance of aeration of the edematous lung. Figures 14d,h,l are the images obtained with symmetric sequences (Figures 14a,e,i) but with the lung boundaries *determined from* the subtraction pictures (Figures 14c,g,k) drawn in. These figures show the potential of *NMR* imaging for performing time-course studies and for obtaining significant physiologic and morphologic information in lungs.

Figure 15 shows the results of our validation experiments (8) in rat lung using the procedure described in Section IV. In order to avoid any errors due to T_2' decay, symmetrical gradients were used. Because of significant variations in water content in different parts of the lung, six different lungs were used, each being sectioned into ten slices. The NMR lung water content for each section of each specimen is plotted on the y-axis and the corresponding gravimetric lung water content on the x-axis. The scatter may also be due to inaccuracies in the gravimetric measurements for thin sections. Nevertheless, the best fit to the data is very close to a straight line of 45° slope through the origin.

ACKNOWLEDGMENT

This research was suported by the U.S. National Institutes of Health under Grant 3-R01-HL-23746-04S1.

REFERENCES

[1] N. C. Staub, *Physiol. Rev.* **54,** 678 (1974).

[2] L. Crooks, *IEEE Trans. on Nuclear Science,* Vol. NS-24 #3, 1239 (1980).

[3] T. A. Case, C. E. Hayes, D. C. Ailion, C. W. Blackburn, C. H. Durney, S. A. Johnson, A. H. Morris, and A. G. Cutillo, to be published.

[4] T. A. Case, D. D. Blatter, D. C. Ailion, C. H. Durney, A. H. Morris, A. G. Cutillo, and S. A. Johnson, to be published.

[5] *CRC Handbook of Chemistry and Physics,* 55th Edition, CRC Press, Cleveland, 1974, pp. E-121 through E-126.

[6] D. D. Blatter, A. H. Morris, D. C. Ailion, A. G. Cutillo, T. A. Case, and D. A. Eckard, submitted to *Invest. Radiol.*

[7] C. E. Hayes, T. A. Case, D. C. Ailion, A. H. Morris, A. G. Cutillo , C. W. Blackburn, C. H. Durney, and S. A. Johnson, *Science* **216,** 1313 (1982).

[8] A. G. Cutillo, A. H. Morris, D. D. Blatter, T. A. Case, D. C. Ailion, C. H. Durney, and S. A. Johnson, *J. Appl. Physiol.* 1984 (in press).